Extraction of Compositional Information for Trafficability Mapping from Hyperspectral Data

Fred A. Kruse* Joseph W. Boardman, and Adam B. Lefkoff
Analytical Imaging and Geophysics
4450 Arapahoe Ave, Suite 100, Boulder, Colorado 80303

ABSTRACT

Trafficability refers to the extent to which the terrain will permit continued movement of any and/or all types of traffic, an issue that ground forces must address in advance of military operations to ensure their success. Multispectral remote sensing technology is currently used by terrain analysts to help assess trafficability, but its utility in producing classical measures of trafficabilty has been limited. This paper describes a hyperspectral trafficability mapping methodology supported by a case history using Airborne Visible/Infrared Imaging Spectrometer (AVIRIS) data. The strong points of the hyperspectral data for trafficability mapping are detection, identification, and mapping of surface composition. Selected spectral libraries were reviewed in the context of trafficability to generate classes of materials with specific trafficability characteristics. These were used in conjunction with scene-based hyperspectral analysis methodologies to produce prototype trafficability products from AVIRIS data. The AVIRIS analysis illustrates that while considerable important information regarding trafficability can be extracted from hyperspectral data, analysis of these data alone can not produce the desired "classical" trafficability products and that data fusion is required to enhance information extracted from hyperspectral data. The principal limitations of hyperspectral data, are 1. That only certain materials have unique spectral features or character that can be detected, 2. that it measures only the very surface and may not be indicative of bulk materials, and 3. That it doesn't provide any textural information, critical for determining classical trafficability measures. Specific additional required information includes terrain information related to topography, and surface texture. This information can be obtained from supporting datasets such as high resolution digital elevation models (DEM), and Synthetic Aperture Radar (SAR).

Keywords: Trafficability, Hyperspectral Mapping, Mineral Identification, Data Fusion

1. INTRODUCTION

Trafficability is the capability of the terrain to bear traffic. It refers to the extent to which the terrain will permit continued movement of any and/or all types of traffic. Cross Country Ground Mobility (Trafficability Factors) include[1]:

- Slope – from digital elevation model (DEM) – 45/30 Degrees for tracked/wheeled, 1.2/0.3m vertical obstacles maximum
- Soil Composition – dry versus wet important, top 0.3 m important – stickiness less important than high centering (sinking), weather can be important factor
- Vegetation – type, trunk thickness (trunk<8 inches for tanks), density/spacing (distance between <4.5 – 6m)
- Man-Made Features – roads/rail lines, obstacles=banks, built up areas, walls, hedgerows, dikes, cuts, fills, urban areas, etc
- Drainage – water barriers (streams, ditches, canals, lakes, marshes, bogs, reservoirs, ponds) (vegetation greenness, density, and size can help indicate)

Some of the above factors can be at least partially addressed using hyperspectral imagery. Hyperspectral data analysis can provide information about the composition and distribution of certain soils, vegetation, manmade materials, and drainage features[2, 3]. The principal limitations of hyperspectral data for trafficability mapping, however, are 1. That only certain materials have unique spectral features or character that can be detected, 2. that it measures only the very surface and may not be indicative of bulk materials, and 3. That it doesn't provide any textural information, critical for determining classical trafficability measures.

This paper summarizes an approach to extracting and categorizing hyperspectral information pertinent to trafficability mapping, principally soil composition as determined from the principal mineralogy. The approach utilizes a scene-based

*Correspondence: Email: kruse@aigllc.com, WWW: http://www.aigllc.com; Telephone: 303-499-9471; FAX: 303-665-6090

methodology – that is, key spectra are located in the hyperspectral data themselves, then compared to spectral libraries for identification and categorization. The image spectra are used to map the distribution and abundance of specific materials important to trafficability. Fusion of other datasets such as digital elevation models is then used to help constrain impediments to trafficability.

2. TRAFFICABILITY CLASSES

Definition of trafficability classes based on mineralogy is key to the above approach. As part of this research, a generalized classification hierarchy based on the principal mineral present in the soil has been designed. The following is an outline of part of this hierarchy. The lower the class number, the higher the concern for trafficability (eg: Trafficability Class I potentially has the greatest negative effect on trafficability).

Trafficability Class I: Montmorillonite Group
Trafficability Class II: Mixed Layer Clays
Trafficability Class III: Illite Group
Trafficability Class IV: Kaolinite Group
Trafficability Class V: Other Clays and Similar Minerals

The following example is for clay mineralogy only, which most directly effects trafficability. Examples of other minerals that may affect trafficability include: micas, chlorites, zeolites, carbonates, silica, Fe-bearing minerals, sulfates and many others.

2.1 Trafficability and Clay Mineralogy (General)

The definition of clay used here is that of mineralogy rather than grain-size. While generally, clays defined by composition will be very fine-grained and principally of clay-size or colloidal particles, clays as defined using spectroscopy or remote sensing may not strictly conform to the < 0.002 mm (2 microns) size. Materials containing high proportions of clay minerals are usually characterized by high plasticity and form a plastic, moldable mass when mixed with water. Plastic clays retain their shape on drying, and become firm, rocklike, and permanently hard on heating or firing. Some clays are nonplastic.

Clays as a group usually have spectral features in the 2.0 – 2.5 μm range. The position of these is dependent on the cations present and the types of molecular bonds[4]. These minerals also typically have prominent spectral features near 1.4 and 1.9 μm that can be detected using field or laboratory spectrometers. Unfortunately, the 1.4 and 1.9 μm features are not useful for remote sensing purposes because of the low atmospheric transmission in these regions.

2.2 Trafficability Class Example: Class I – Montmorillonite Group

The following example is provided to illustrate the general information format compiled for each trafficibility class and the key factors for this specific group.

Trafficability Class I: Montmorillonite Group Minerals –"Smectites" (Montmorillonite, Hectorite, Nontronite, Saponite, Sauconite): A group of expanding-lattice clay minerals characterized by a three-layer crystal lattice (one sheet of aluminum and hydroxyl between two sheets of silicon and oxygen. They are subject to high cation exchange capacities, and to swelling on wetting (and shrinking on drying) due to introduction of considerable interlayer water. Key Spectral Features: 2.2 μm region for montmorillonite, 2.3 μm region for others (also strong 1.4 and 1.9 μm in field and lab spectra for all group members). Figure 1 shows an example of reflectance spectra for minerals in this class.

Effects on trafficability include:
Loss of traction when wet - Sinking
Loss of traction when wet - Stickiness
Reduced soil permeability (increased chance of marshy conditions)
Potential slope differences
Potential vegetation differences

Spectral Libraries: USGS, JPL, JHU, IGCP264

Summary and Caveats: All clay-bearing soils can reduce cross country trafficability. Montmorillonite group clays and mixed-layer clays are the biggest potential problems, as they absorb water under high moisture conditions. Spectral detection

of clay mineralogy using remote sensing instruments is generally not sufficient to fully determine trafficability, as this only applies to the first approximately 50 microns of the surface. Abundance estimates determined by linear spectral unmixing or other means may assist in determining areas with high probability of reduced trafficability, again however, these abundances correspond only to the optically dominant material. This does not necessarily correspond to the abundance of the material as measured by traditional volumetric means (weight-percent).

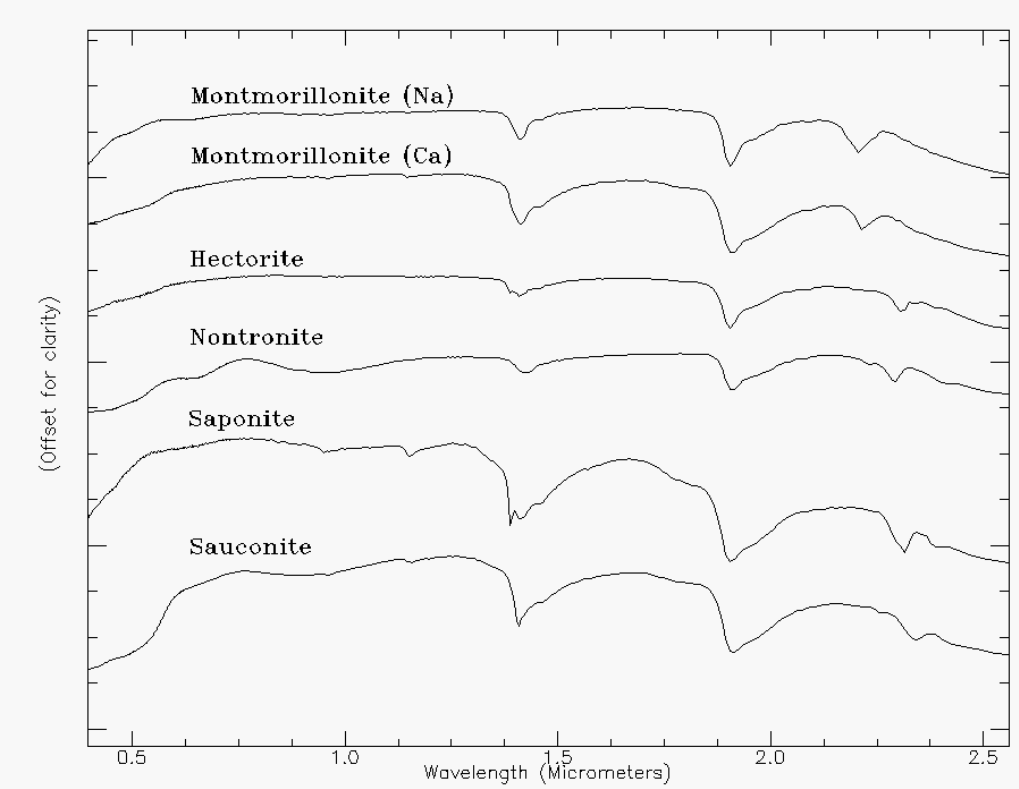

Figure 1: Montmorillonite Group Minerals –"Smectites"

3. METHODOLOGY

The following general methodology was followed to help assess trafficability using hyperspectral data:

- Analysis of spectral libraries in the context of trafficability: Minerals and other materials were grouped to define trafficability classes. Key spectral features for mapping specific trafficablity classes were defined
- Analyze hyperspectral data and determine mineralogy on per-pixel-basis
- Combine minerals identified into trafficability classes as previously defined
- Produce map of hyperspectral trafficability classes
- Augment with textural information derived from other sources such as digital elevation models (DEMs) and Synthetic Aperture Radar (SAR)

3.1 Per-Pixel Hyperspectral Analysis

Methods being used in the analysis include reduction to apparent reflectance using ATREM[5], spectral data reduction using the Minimum Noise Fraction (MNF) transformation[6], spatial data reduction using the Pixel Purity Index™ (PPI)[7], an n-Dimensional Visualizer™ to determine image endmembers[6, 7], identification of endmembers using their reflectance spectra[7, 8] in the Spectral Analyst™, and mineral mapping using Mixture-Tuned Matched Filtering[11]. Figure 2 is a diagram showing the processing procedures.

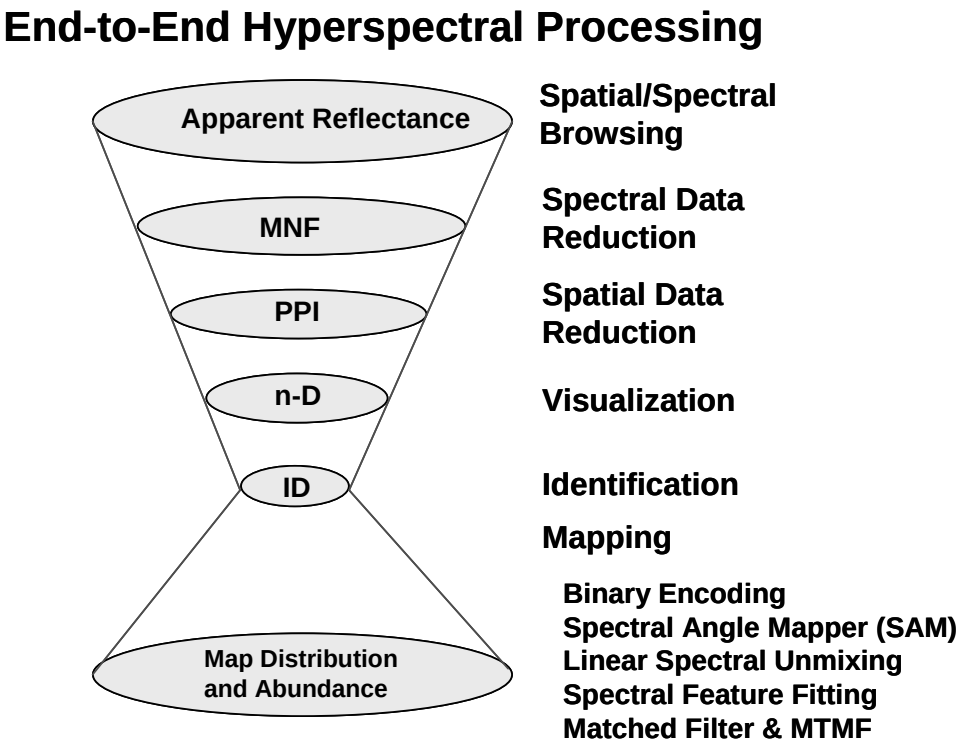

Figure 2 AIG Standardized Processing methods for hyperspectral data analysis.

3.1.1 Atmospheric Correction using ATREM

Remote sensing measurements of the Earth's surface are strongly influenced by the atmosphere[12]. Both scattering and absorption by gases and particulates affect the amount and wavelengths of light reaching the sensors. Absorption by atmospheric gases is dominated by water vapor with smaller contributions from carbon dioxide, ozone, and other gases[13] Strong atmospheric water absorption bands make the atmosphere opaque in many regions (for example the 1.4 and 1.9 μm regions) and only small atmospheric windows are available for terrestrial remote sensing.

The most critical step in most imaging spectrometer data analysis strategies is to convert the data to reflectance (or emissivity for MWIR/LWIR), principally so that individual spectra can be compared directly with laboratory or field data for identification. (If comparison to reflectance/emissivity isn't required, then this step may be eliminated, but for most work, this is a requirement). This means that accurate wavelength calibration be performed. Laboratory measurements made before and after data acquisition usually provide the initial wavelength calibration. An additional check on the wavelength calibration can be made by comparing the positions of known atmospheric absorption features to their locations in the imaging spectrometer data. Atmospheric carbon dioxide (CO_2) absorption bands located at 2.005, and 2.055 μm are useful for wavelength-calibration of the data in the shortwave infrared[14, 15]. In the visible and near-infrared portion of the spectrum, narrow atmospheric water bands at 0.69, 0.72, and 0.76 μm can be used to calibrate wavelengths. Ideally, imaging spectrometer data should be calibrated to absolute reflectance using onboard calibration. In the absence of onboard calibration, model-based methods should be used. A radiative transfer model-based technique the "Atmospheric Removal Program" (ATREM)[5] developed by the Center for the Study of Earth from Space (CSES) at the University of Colorado, Boulder, using 224-channel Airborne Visible/Infrared Imaging Spectrometer (AVIRIS) allows inversion of hyperspectral data to apparent reflectance without *a priori* knowledge. The ATREM method involves using a three-channel ratioing approach that utilizes the 0.94 and 1.1 μm water vapor bands to calculate water vapor on a pixel-by-pixel basis from the AVIRIS data. Apparent reflectance spectra are first obtained by dividing each AVIRIS spectrum by the solar irradiance curve above the atmosphere[13]. A number of theoretical water vapor transmittance spectra for the 0.94 and 1.1 μm water vapor bands are calculated for varying amounts of atmospheric water vapor using an approximate radiative transfer code called "Simulation of the Satellite Signal in the Solar Spectrum (6S)[16] and a narrow band spectral model[17]. The modeled spectra are run through the three-channel ratioing method to generate a lookup table of water vapor concentrations that can be

used to convert the AVIRIS apparent reflectance measurements to total column water vapor. The output of this procedure is an image showing the spatial distribution of various water vapor concentrations as derived for each pixel of the AVIRIS data. The water vapor image is then used along with transmittance spectra derived for each of atmospheric gases CO_2, O_3, N_2O, CO, CH_4, and O_2 using the narrow band model and 6S model to produce scaled surface reflectance[5]. This model-based technique produces total water vapor column images and reflectance calibrated AVIRIS data without a priori knowledge.

With the currently available atmospheric correction models, we have overcome one of the major barriers to widespread use and analysis of hyperspectral data. These methods make it possible to quantitatively derive physical parameters and analyze data from different regions and different times without a priori knowledge. We can also compare and analyze imaging spectrometry data acquired by different instruments, compare to field and laboratory spectral measurements, or to spectra generated using theoretical models.

3.1.2 Spectral Data Reduction: The MNF Transformation

The inherent dimensionality of the data is determined using a special orthogonalization procedure related to principal components, the Minimum Noise Fraction (MNF) transform[6]. The MNF transformation is used to determine the inherent dimensionality of the data, to segregate noise in the data, and to reduce the computational requirements for subsequent processing[6, 18]. The MNF transformation can be used to partition the data space into two parts: one associated with large eigenvalues and coherent eigenimages, and a second with near-unity eigenvalues and noise-dominated images. The noise in the resulting data set has a Gaussian distribution and unit variance. Eigenvalues resulting from the MNF transform describe the intrinsic dimensionality of the data set; i.e., the number of spectral endmembers that account for the majority of the spectral variability in the scene[18]. By using only the coherent portions in subsequent processing, the noise is separated from the data, thus improving spectral processing results. Based on combined examination of the eigenvalues and eigenimages (MNF results), the lower order MNF bands are discarded and the most significant MNF bands are selected for further processing.

3.1.3 Spatial Data Reduction: The Pixel Purity Index™ (PPI)

After the MNF transform, the significant bands of the transformed data are be subjected to a "Pixel Purity Index (PPI)" investigation, designed to locate the most spectrally extreme (unique or different or "pure") pixels[7]. The most spectrally pure pixels typically correspond to mixing endmembers. The PPI is computed by repeatedly projecting n-dimensional scatterplots onto a random unit vector. The extreme pixels in each projection are recorded and the total number of times each pixel is marked as extreme is noted. A PPI image is created in which the digital number of each pixel corresponds to the number of times that pixel was recorded as extreme. A histogram of these images shows the distribution of "hits" by the PPI. A threshold is interactively selected using the histogram and used to select only the purest pixels in order to keep the number of pixels to be analyzed to a minimum. These pixels are used as input to an interactive visualization procedure for separation of specific endmembers.

3.1.4 Interactive Visualization: The n-Dimensional Visualizer™

An interactive "n-Dimensional" visualization technique is used to extract the endmember spectra using the spectral mixing space. Utilizing a geometric model, spectra are thought of as points in the n-dimensional scatterplot, where n is the number of bands[7, 8]. The coordinates of the points in n-space consist of "n" values that are simply the spectral reflectance values in each band for a given pixel. The distribution of these points in n-space can be used to estimate the number of spectral endmembers and their pure spectral signatures. This geometric model provides an intuitive means to understand the spectral characteristics of materials. Pure endmembers occur at the vertices of the geometric figure. Mixtures occur either along the edges (2 endmembers), on one of the faces (3 endmembers inside a triangle, 4 inside a tetrahedron, and so on), or in the interior of the geometric figure (multiple endmembers). This methodology has been implemented as the "n-Dimensional Visualizer™" in the ENVI software.

3.1.5 Feature-Based Identification: The ENVI Spectral Analyst™

Many methods used for analysis of hyperspectral data, while finding unique materials in the data, or matching library spectra to image spectra, do not directly identify specific materials. Techniques for direct identification of materials, however, via extraction of spectral features from field and laboratory reflectance spectra and hyperspectral data have been in use for some time[9, 10, 19, 20, 21, 22, 23, 24, 25, 26]. Most recently, some of these methods have been applied to military problems (Kruse and Lefkoff, unpublished data), and work has begun to extend these algorithms to the MWIR and TIR (Kruse, unpublished data). Similar feature-based analysis procedures have also been at least partially implemented in the "Bands" algorithm being developed by NAIC.

The ENVI Spectral Analyst™ helps to identify materials based on their spectral characteristics. It uses spectral matching techniques, such as binary encoding, spectral angle mapper, and spectral feature fitting to rank the match of an unknown spectrum to the materials in a spectral library. Users can also define their own spectral similarity techniques and add them to the Spectral Analyst. The output of the Spectral Analyst is a list of the materials in the input spectral library ranked in order of best to worst match. An overall similarity "score", and individual 0 to 1 scores for each method are reported. Users have the option of comparing the unknown spectrum to any of the matched reference spectra in a spectral plot. The Spectral Analyst is meant as a starting point to put users on the right track towards identifying the materials in an image scene. Used properly and with a good spectral library, it can provide excellent suggestions for identification.

3.1.6 Spectral Mapping Using Mixture-Tuned Matched Filtering (MTMF)™

Once the endmembers have been extracted and identified, then their occurrence and abundances can be mapped on a per-pixel basis. Mixture-Tuned Matched Filtering (MTMF)[11] is a hybrid spectral mapping method based on the combination of well-known signal processing methodologies[27, 28] and linear mixture theory[7, 8]. The Matched Filter (MF) portion of the algorithm maximizes the response of a known endmember and suppressing the response of the composite unknown background[27, 28]. Mixture-Tuning uses linear spectral mixing theory to constrain the result to feasible mixtures and reduce false alarm rates[11] (Figure 3).

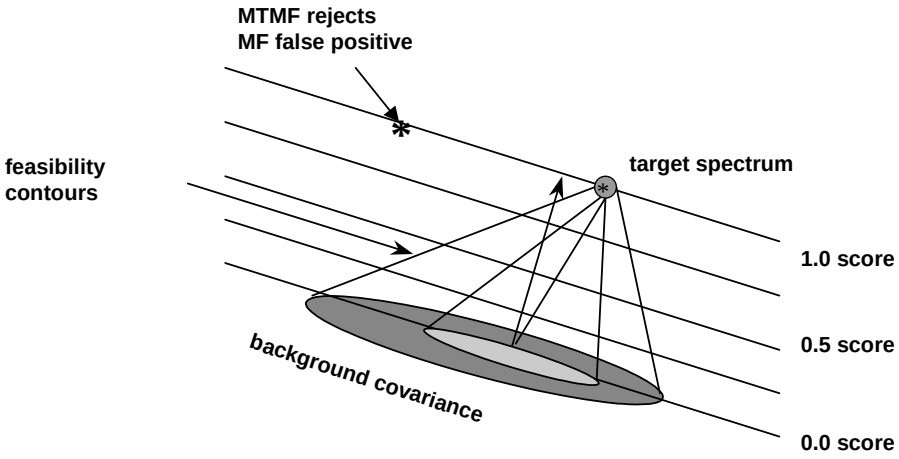

Figure 3: Diagram illustrating the MTMF

The Mixture-Tuned-Matched Filter preserves the ease of calculation of the MF and allows for unambiguous target selectivity (reduced false alarms), impossible with a simple MF alone[10]. The MTMF method recognizes that targets are replacing background signature in a pixel, not adding to it, as has often been proposed for MF methods. This fact requires that linear spectral mixing be considered. If all the scene endmembers are accurately known, a mixing model would give better detection than a simple MF. In practice, however, it is usually unreasonable to assume that all background endmembers are known. MTMF combines the statistical method of the MF with the deterministic method of the linear mixing model. The one known endmember is the known target of interest. The background statistics are used, just as in MF, to define the variability in the unknown natural and dominant endmembers. The known signature of the target material is used to define one corner of a mixing simplex, a fixed point with a well-known noise distribution. The background covariance (or equivalently eigenvectors and eigenvalues) gives the shape, orientation and size of the background spectral scatter. Because the data have been whitened and decorrelated using the Minimum Noise Fraction (MNF) transform, the distribution about a known point is just a unit variance isotropic Gaussian distribution. The MF vector and associated scores are calculated using standard methods. The MTMF calculation includes an additional parameter, an “infeasibility” measure, describing how likely it is that each pixel is a mixture of our known target and the background materials (Figure 3). “Hypercones” of equal probability converging on the target spectrum and diverging away to meet the background distribution describe the feasibility of the mixture of target and background (Figure 3). To get the infeasibility score for a certain pixel, first its MF is found, then its distance from the line that connects the mean of the background and the target is measured. This measurement is done in the plane of the fixed MF score and is done in terms of number of infeasibility standard deviations for that MF score. A pixel outside the feasibility hypercone, although it does still get a perfect MF score, is shown to be a false positive because it is highly infeasible as a mixture of the target spectrum and the background distribution.

4. RESULTS

The above methods were applied to AVIRIS data of a site near Hanover, Colorado. AVIRIS is a 224 spectral band hyperspectral sensor with 30 m spatial pixels[29, 30]. Operationally, the data were converted to apparent reflectance (Figure 4), then the last 60 AVIRIS bands (1.92 – 2.51 μm) were linearly transformed using the MNF transformation (Figure 4), and the top MNF bands, which contain most of the spectral information, were used to determine the most likely endmembers using the PPI procedure (Figure 5). These potential endmember spectra were loaded into an n-dimensional scatterplot and rotated in real time on the computer screen until "points" or extremities on the scatterplot were exposed (Figure 5). These projections were "painted" using Region-of-Interest (ROI) definition procedures and then rotated again in 3 or more dimensions (3 or more bands) to determine if their signatures were unique in the AVIRIS MNF data. Once a set of unique pixels were defined, then each separate projection on the scatterplot (corresponding to a pure endmember) was exported to a ROI in the image. Mean spectra were then extracted for each ROI from the apparent reflectance data to act as endmembers for spectral mapping (Figure 5). These endmembers were identified using the Spectral Analyst and grouped according to mineralogy into one of the pre-defined trafficability classes (Figure 6). A subset of these endmembers were used for subsequent classification and other processing. MTMF was used to produce mineral abundance maps (Figure 7). The results are generally presented as gray-scale images with values from 0 to 1.0, which provide a means of estimating mineral abundance. Brighter pixels in the images represent higher mineral abundances. These can then be combined as color-coded images or thematic image maps to show the distribution of principal mineralogies (Figure 8).

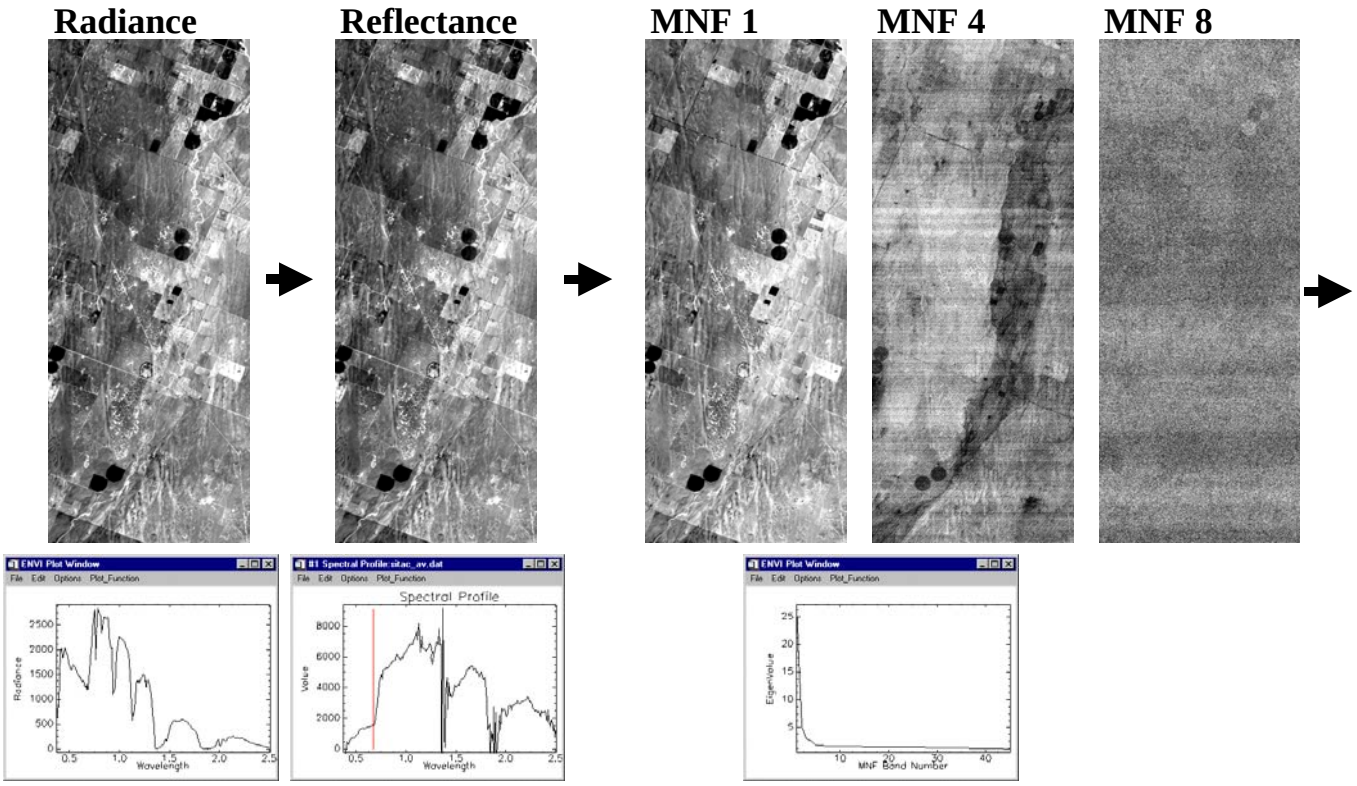

Figure 4: Analysis of Hanover, Colorado, AVIRIS data included correction from radiance to apparent reflectance (left) and spectral reduction using the MNF transform (right). Plots are from left to right: Radiance, Reflectance, and MNF Eigenvalues.

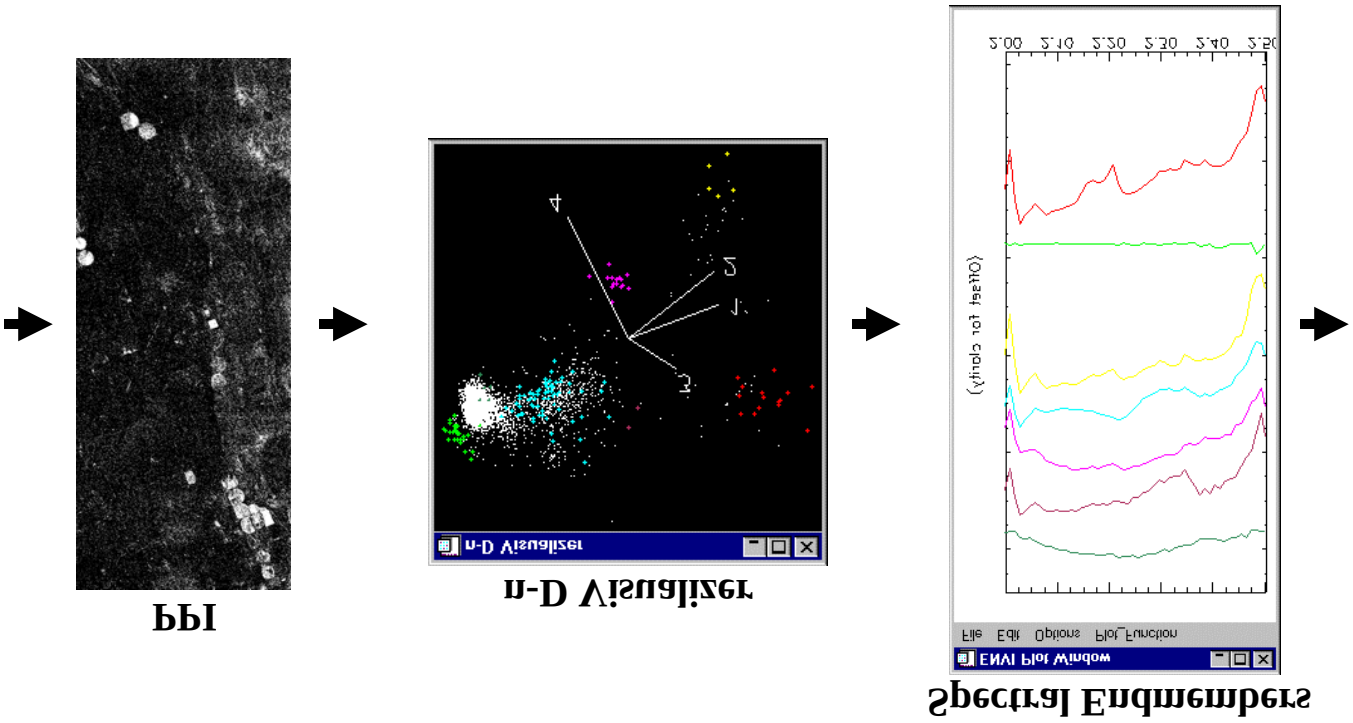

Figure 5: The next step in the analysis of Hanover, Colorado, AVIRIS data included extraction of pure pixels using the Pixel Purity Index (PPI, left), determination of endmembers using the n-D Visualizer (center), and extraction of endmember spectra from the apparent reflectance data (right).

SpectralAnalyst

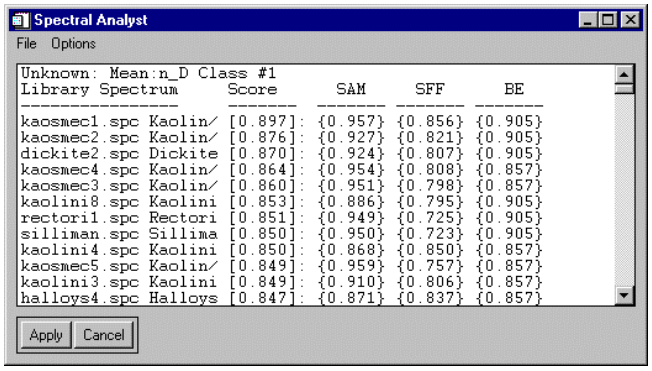

Trafficability Class

- **Trafficability Class IV:** **Kaolinite Group Minerals** (Kaolinite, Dickite, Endellite, Haloysite, Nacrite): The kaolin minerals are generally derived from alteration of alkali feldspars and micas. They absorb less water than montmorillonite and illite, and thus have lower plasticity indexes, lower liquid limits, and less shrinkage when drying from a wet state. Key Spectral Features: Doublet at 2.16/2.2 µm, with relative strengths dependent on species (also doublet at 1.4 µm in field and laboratory spectra)

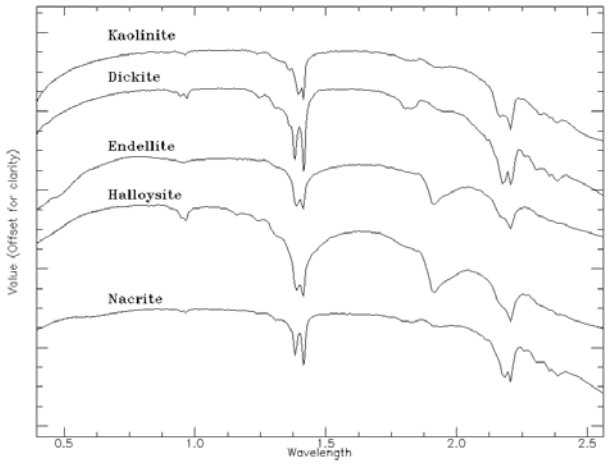

Figure 6: Identification of endmember spectra using the Spectral Analyst (left) and grouping into appropriate trafficability classes (right).

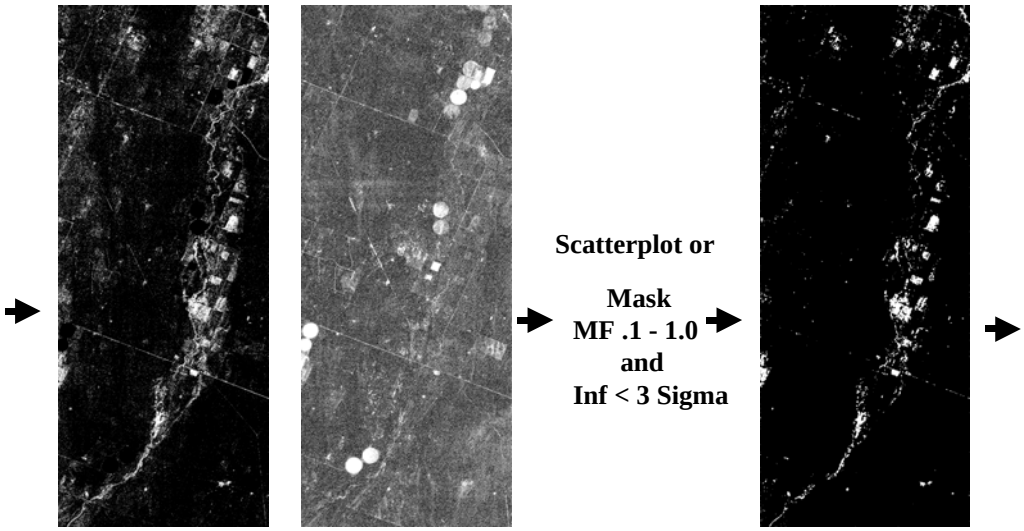

Figure 7: Spectral mapping using Mixture-Tuned-Matched Filtering (left), and thresholding using both the Matched Filter score and Infeasibility score (right).

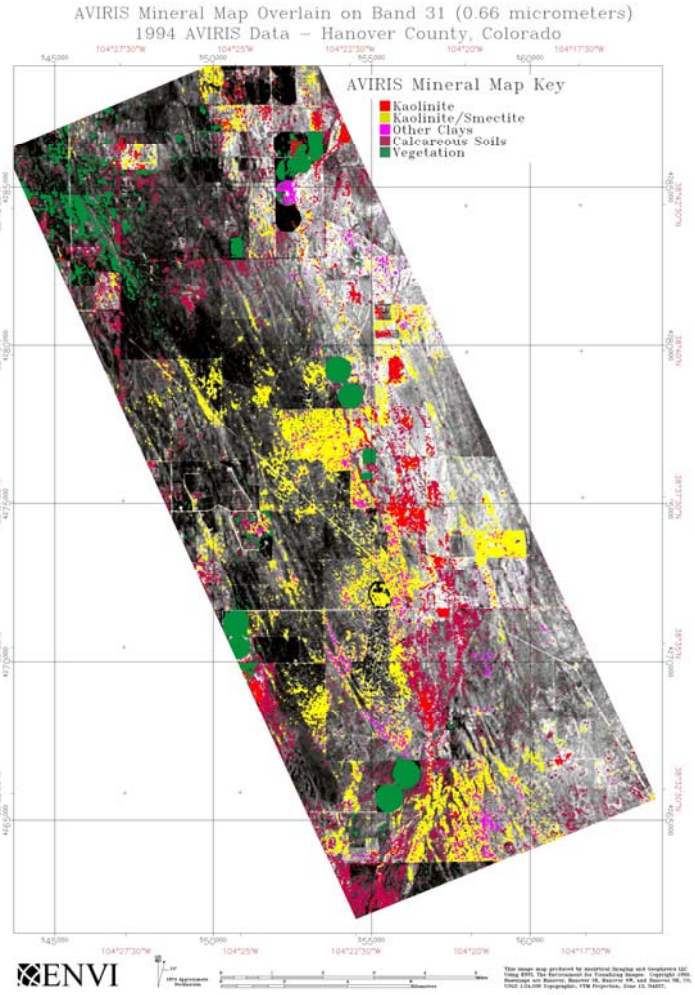

Figure 8: Sample hyperspectral-derived mineral map product. Additional information is required to convert to conventional trafficability map.

It is easily seen that the information provided by the hyperspectral data as shown in Figure 8 is inadequate to fully define trafficability parameters. Specifically, the texture and morphology of the terrain is not taken into consideration. This can have a negative effect on identification of areas of restricted trafficability. For example, an area that is covered by clay, but that occurs in a flat field is probably not important, whereas a steep slope covered by clay may cause trafficability restrictions. The best way to inprove discrimination of low trafficability areas is to use data fusion. In this case, a digital elevation model of the area was used to identify those areas with high slopes. These were then compared using a logical AND to identify areas that have both a high clay content, and high slopes (Figure 9.)

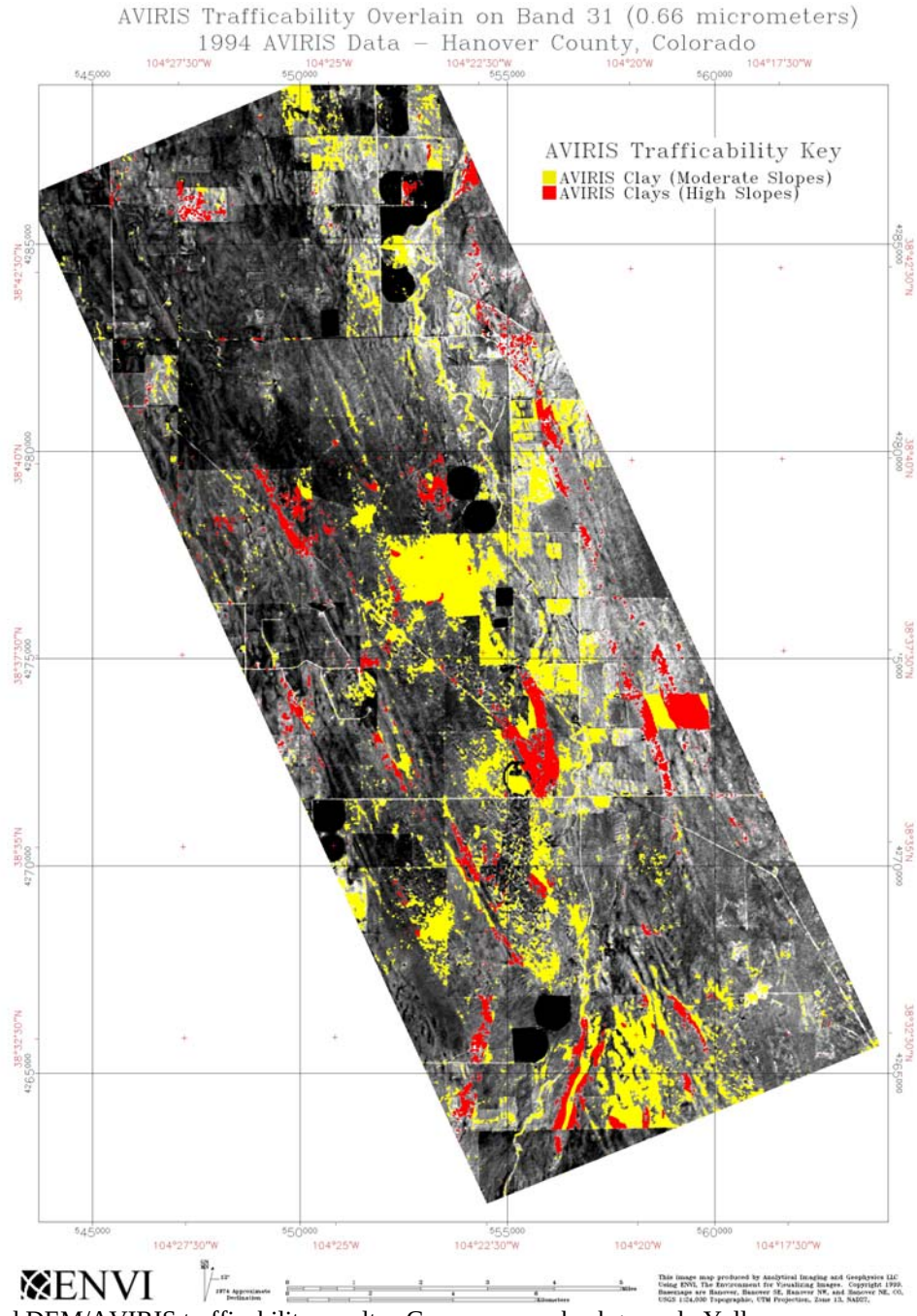

Figure 9: Combined DEM/AVIRIS trafficability results. Gray areas are background. Yellow areas are moderate slopes with clay. Red areas are high slopes with clay.

5. CONCLUSIONS

We have shown that the AIG approach to hyperspectral analysis is effective for detecting, characterizing, identifying and geolocating selected materials important to trafficablity mapping. This methodology follows the "standardized" hyperspectral approach advocated by AIG, including correction to apparent reflectance using an atmospheric model (ATREM), spectral data reduction and separation of signal from noise using the Mininmum Noise Transform (MNF), selection of key pixels that can explain the data via a mixing model using the Pixel Purity Index (PPI), identification of materials using spectral matching to a library, and mapping using the Mixture-Tuned Matched Filtering approach. Grouping of specific minerals into classes important to trafficability is new to this application. Hyperspectral data can make a significant contribution to mapping trafficability, however, it is limited in its application to classical trafficability measures by the lack of textural and contextural information. We've demonstrated that hyperspectral data alone can not produce all of the required information. An example using slope derived from DEM data demonstrates the viability of using fused datasets to produce improved trafficability maps.

The principal benefits of using hyperspectral data for trafficablity analysis, are:

- Detailed surface compositional information that can not be obtained elsewhere
- Complete area coverage without extensive ground work

The principal limitations of using hyperspectral data for trafficablity analysis, are:

- That only certain materials have unique spectral features or character that can be detected. These do not necessarily relate to materials critical for trafficabiltiy determinations
- That it measures only the very surface and may not be indicative of bulk materials
- That it doesn't provide any textural information, critical for determining classical trafficability measures.

Key Findings of the Research include:

- Prototype Hyperspectral Trafficability Mapping Methodology
- Simple data-fusion approaches for enhanced mapping
- Hanover, Colorado, Trafficability Case History

6. ACKNOWLEDGMENTS

This research was supported by the Spectral Information Technology Center (SITAC) under the HYMYSMO program. Development of the Spectral Analyst and MTMF procedures was partially supported by U. S. Army Topographic Engineering Center.

7. REFERENCES

1. US Army Field Manual, FM 5-36, 1985, Route Reconnaissance and Classification: Headquarters, Department of the Army, Washington, DC, p. 6-1 – 6-24.
2. Kruse, F. A., Boardman, J. W., and Huntington, J. F., 1999a, Fifteen Years of Hyperspectral Data: northern Grapevine Mountains, Nevada: in Proceedings of the 8th JPL Airborne Earth Science Workshop: Jet Propulsion Laboratory Publication, JPL Publication 99-17, p. 247 - 258.
3. Johnson, A. J., Windesheim, E., and Brockhaus, J., 1998, Hyperspectral Imagery for Trafficability Analysis: Proceedings of the 1998 IEEE Aerospace Conference, Snowmass, Colorado, February 1998, on CD-ROM, paper Fp247, IEEE.
4. Clark, R. N., T. V. V. King, M. Klejwa, and G. A. Swayze, 1990. High spectral resolution spectroscopy of minerals: J. Geophys. Res., 95 (B8), 12653 - 12680.
5. Center for the Study of Earth from Space (CSES), 1999, Atmosphere REMoval Program (ATREM) User's Guide, Version 3.1, Center for the Study of Earth from Space, Boulder, Colorado, 31 p.
6. Green, A. A., Berman, M., Switzer, B., and Craig, M. D., 1988, A transformation for ordering multispectral data in terms of image quality with implications for noise removal: IEEE Transactions on Geoscience and Remote Sensing, v. 26, no. 1, p. 65 - 74.
7. Boardman, J. W., Kruse, F. A., and Green, R. O., 1995, Mapping target signatures via partial unmixing of AVIRIS data: in Summaries, Fifth JPL Airborne Earth Science Workshop, JPL Publication 95-1, v. 1, p. 23-26.
8. Boardman, J. W., 1993, Automated spectral unmixing of AVIRIS data using convex geometry concepts: in Summaries, Fourth JPL Airborne Geoscience Workshop
9. Kruse, F. A., Lefkoff, A. B., and Dietz, J. B., 1993, Expert System-Based Mineral Mapping in northern Death Valley, California/Nevada using the Airborne Visible/Infrared Imaging Spectrometer (AVIRIS): Remote Sensing of Environment, Special issue on AVIRIS, May-June 1993, v. 44, p. 309 - 336.
10. Kruse, F. A., and Lefkoff, A. B., 1993, Knowledge-based geologic mapping with imaging spectrometers: Remote

Sensing Reviews, Special Issue on NASA Innovative Research Program (IRP) results, v. 8, p. 3 - 28.
11. Boardman, J. W., 1998, Leveraging the high dimensionality of AVIRIS data for improved sub-pixel target unmixing and rejection of false positives: mixure tuned matched filtering, in: Summaries of the Seventh Annual JPL Airborne Geoscience Workshop, Pasadena, CA, p. 55.
12. Goetz, A. F. H., Vane, G., Solomon, J. E., and Rock, B. N., 1985, Imaging spectrometry for earth remote sensing: Science, 228, 1147-1153.
13. Gao B. and Goetz, A. F. H., 1990, Column atmospheric water vapor and vegetation liquid water retrievals from airborne imaging spectrometer data: Journal of Geophysical Research, v. 95, no. D4, p. 3549-3564.
14. Kneisyz, F. X., Shettle, E. P., Abreau, L. W., Chetwynd, J. H., Anderson, G. P., Gallery, W. O., Selby, E. A., and Clough, S. A., 1988, Users guide to LOWTRAN 7, AFGL-TR-8-0177, Airforce Geophysics Laboratory, Bedford, MA.
15. Vane, Gregg, 1987, First results from the Airborne Visible/Infrared Imaging Spectrometer (AVIRIS): in Proceedings, 31st Annual International Technical Symposium, Society of Photo-Optical Instrumentation Engineers, v. 834, p. 166-174.
16. Tanre, D., Deroo, C., Duhaut, P., Herman, M., Morchrette, J. J., Perbos, J., and Deschamps, P. Y., 1986, Simulation of the Satellite Signal in the Solar Spectrum (5S), Users's Guide (U. S. T. de Lille, 59655 Villeneuve d'ascq, France: Laboratoire d'Optique Atmospherique).
17. Malkmus, W., 1967, Random Lorentz band model with exponential-tailed S line intensity distribution function: J. Opt. Soc. Am., v 57, p. 323-329.
18. Boardman J. W., and Kruse, F. A., 1994, Automated spectral analysis: A geologic example using AVIRIS data, north Grapevine Mountains, Nevada: in Proceedings, Tenth Thematic Conference on Geologic Remote Sensing, Environmental Research Institute of Michigan, Ann Arbor, MI, p. I-407 - I-418.
19. Green, A. A., and Craig, M. D., 1985, Analysis of aircraft spectrometer data with logarithmic residuals: in Proceedings, AIS workshop, 8-10 April, 1985, JPL Publication 85-41, Jet Propulsion Laboratory, Pasadena, California, p. 111-119.
20. Kruse, F. A., Raines, G. L., and Watson, Kenneth, 1985, Analytical techniques for extracting geologic information from multichannel airborne spectroradiometer and airborne imaging spectrometer data: in Proceedings, International Symposium on Remote Sensing of Environment, Fourth Thematic Conference, "Remote Sensing for Exploration Geology", San Francisco, California, 1-4 April, 1985, p. 309-324.
21. Yamaguchi, Yasushi, and Lyon, R. J. P., 1986, Identification of clay minerals by feature coding of near-infrared spectra: in Proceedings, International Symposium on Remote Sensing of Environment, Fifth Thematic Conference, "Remote Sensing for Exploration Geology", Reno, Nevada, 29 September- 2 October, 1986, Environmental Research Institute of Michigan, Ann Arbor, p. 627-636.
22. Clark, R. N., King, T. V. V., and Gorelick, N. S., 1987, Automatic continuum analysis of reflectance spectra: in Proceedings, Third AIS workshop, 2-4 June, 1987, JPL Publication 87-30, Jet Propulsion Laboratory, Pasadena, California, p. 138-142.
23. Kruse, F. A., Calvin, W. M., and Seznec, O., 1988, Automated extraction of absorption features from Airborne Visible/Infrared Imaging Spectrometer (AVIRIS) and Geophysical Environmental Research imaging spectrometer (GERIS) data: In Proceedings of the Airborne Visible/Infrared Imaging Spectrometer (AVIRIS) performance evaluation workshop, JPL Publication 88-38, p. 62-75.
24. Kruse, F. A., 1988, Use of Airborne Imaging Spectrometer data to map minerals associated with hydrothermally altered rocks in the northern Grapevine Mountains, Nevada and California: Remote Sensing of Environment, v. 24, no. 1, pp. 31-51.
25. Clark, R. N., Swayze, G. A., Gallagher, A., Gorelick, N., and Kruse, F. A., 1991, Mapping with imaging spectrometer data using the complete band shape least-squares algorithm simultaneously fit to multiple spectral features from multiple materials: in Proceedings, 3rd Airborne Visible/Infrared Imaging Spectrometer (AVIRIS) workshop, JPL Publication 91-28, p. 2-3.
26. Kruse, F. A., 1995, Mapping spectral variability of geologic targets using Airborne Visible/Infrared Imaging Spectrometer (AVIRIS) data and a combined spectral feature/unmixing approach: in Proceedings, AeroSense'95, SPIE, 17-21 April 1995, Orlando, Florida.
27. Chen, J. Y. and I. S. Reed, 1987, A detection algorithm for optical targets in clutter, IEEE Trans. on Aerosp. Electron. Syst., V. AES-23, No. 1.
28. Harsanyi, J. C., and Chang, C. I., 1994, Hyperspectral image classification and dimensionality reduction: An orthogonal subspace projection approach: IEEE Trans. Geosci. and Remote Sens., v. 32, p. 779-785.
29. Porter, W. M., and Enmark, H. E., 1987, System overview of the Airborne Visible/Infrared Imaging Spectrometer (AVIRIS), in Proceedings, Society of Photo-Optical Instrumentation Engineers (SPIE), v. 834, p. 22-31
30. Green, R. O., Pavri, B., Faust, J., Chovit, C., and Williams, O., 1999, AVIRIS in-flight radiometric calibration results for 1998: in Proceedings of the 8th JPL Airborne Earth Science Workshop: JPL Publication 99-17, p. 161 – 176.